Int J Adv Manuf Technol (2018) 95:1377–1397
https://doi.org/10.1007/s00170-017-1322-x

ORIGINAL ARTICLE

Friction stir forming of dissimilar grade aluminum alloys: Influence of tool rotational speed on the joint evolution, mechanical performance, and failure modes

Tinu P. Saju [1] · **R. Ganesh Narayanan** [1]

Received: 12 December 2016 / Accepted: 2 November 2017 / Published online: 10 November 2017

Abstract Friction stir forming (FSF) is a solid-state, eco-friendly spot welding technique primarily applied for lap joining dissimilar sheet metals. The details related to the process are scarce in literature. The present work explores the potential of the FSF process for joining dissimilar grade alloys of same metal, namely aluminum. The effect of tool rotational speed on the joint formation and mechanical performance of FSF joints between AA5052-H32 and AA 6061-T6 sheets is studied through systematic experimentation and macrostructure analysis. Hardness distribution across the joint, joint morphology, and failure modes at varying rotational speeds are also presented. The tool rotational speed shows significant effect on the mechanical performance results, zones formed within the joint, and hardness distribution across the joint. Maximum lap shear strength, about 6 kN, obtained in the present work is superior than that of joints fabricated on same material combination with other friction-based joining technologies. The lower and medium tool rotational speeds, between 500 and 1500 rpm, are the best choices for fabricating FSF joints for the materials used. Macrostructure analysis revealed that at lower tool rotational speed (< 1500 rpm), continuous stir zone is observed, at medium tool rotational speed (1500 rpm), partitions within the stir zone are visible, and at higher tool rotational speed (> 1500 rpm), localized stir zones are distributed over the cross-section. Friction stir form samples showed an inverted "W"-shaped hardness profile over the cross-section, and the joint morphological features are independent of the tool rotational speed. Failure modes such as partial bond delamination, tear-off, and pull-out occur randomly and have no systematic correlation with the tool rotational speed.

Keywords Friction stir forming · Tool rotational speed · Aluminum alloy · Lap shear test · Pin-less tool · Failure modes

1 Introduction

In the past decade, solid-state welding techniques have acquired the attention of manufacturing industry due to its inherent advantages, ease of operation, and its ability to emerge as alternative joining solutions. Processes using joining by plastic deformation principle, like mechanical clinching and self-pierced riveting (SPR), became commercially popular. However, they possess disadvantages like split, lack of mechanical interlocking, and neck fracture, due to the severe plastic deformation in the joint zone [1]. SPR requires double-sided accessibility and piercing of upper sheet, which introduces weak zones that can grow into cracks, while loading. Use of mechanical clinching is affected by vibration and poor esthetic appearance such as downward protrusion of the lower sheet and limited use on the sliding surfaces and visible areas.

Friction stir welding (FSW) is the first eco-friendly solid-state joining process, using stir friction heat, invented by TWI, England, in 1991 [2]. Since welding of aluminum using conventional techniques is a problematic issue, initial attempts of FSW were concentrated on joining aluminum and its alloys. The process was later utilized for joining iron-based alloys such as stainless steel [3]. More detailed understanding regarding mechanisms governing friction-based processes were obtained through three dimensional finite element simulations

✉ R. Ganesh Narayanan
ganu@iitg.ernet.in

Tinu P. Saju
tinu.saju@iitg.ernet.in

[1] Department of Mechanical Engineering, Indian Institute of Technology Guwahati, Assam 781039, India

based on solid mechanics, where material flow, material deformations, and formation of weld zones were revealed [4]. Many variants for FSW were developed over the past two decades including Friction stir processing, Friction stir spot welding, Friction welding, and many more.

Friction stir processing (FSP) has emerged as a generic metal working technique where surface modification and material transfer are possible with the use of a friction stir tool. The common friction stir processing techniques such as friction stir surface modification (enhancing the properties of the work metal surface), friction stir deposition (depositing hot plasticized stir tool metal at localized defective zones of another work metal surface), and friction stir surfacing (metal transfer from the end of a consumable stir tool creates a coating over the work metal surface, while stirring) are under research. The following works regarding FSP techniques show the effectiveness of a friction stir tool to enhance the qualities of the work piece surface. A significant microstructural refinement, densification, and homogeneity in the processed zone were obtained in AA7075Al-T651 at 400 rpm tool rotation speed and 102 mm/min transverse speed through friction stir surface modification [5]. High strain rate superplastic elongations were observed in friction stir-processed AA7075Al with a grain size of 3.8 μm [6] and friction stir-processed magnesium alloy AZ31, which possess remarkable grain refinement and second phase particle dissolution [7]. The incorporation of the ceramic particles into the metallic substrate plate is possible through friction stir surfacing. Al-SiC surface composites with the surface composite layer thickness ranging up to 200 μm were successfully fabricated through friction stir surfacing [8]. The microstructure of heterogeneous powdered metallic materials such as cast alloys, metal matrix composites, and nano-phase aluminum alloys can be modified by using a threaded friction stir tool. Coarse acicular Si particles were broken and uniformly dispersed, and healed the casting porosity through FSP, which led to a significant improvement in both strength and ductility of aluminum matrix in A356 plates [9]. Fabrication of ultra-fine-grained Al-Al_2Cu composite [10], aluminum reinforced with nanometer-sized Al_3Ti particles [11], and the fabrication of multi-elemental Mg-Al-Zn intermetallic alloys from thin foils of AZ31, Al, and Zn [12] were done through in-situ FSP. Incorporation of carbon nanotubes into copper substrate through FSP enhanced the microhardness and wear resistance of pure copper [13]. Welding of non-flat surfaces such as dissimilar thin-walled pipes made of aluminum alloy and austenitic stainless steel is also possible with solid-state welding namely friction welding, where the need of a stir tool is eliminated [14].

Sheet metals can also be lap joined, utilizing local extrusion forging, by virtue of stir friction heat. Friction stir forming (FSF) is such a thermo-mechanical process by which lap joints are produced in similar and dissimilar sheet metal combinations through simultaneous stir heating and plastic deformation. Friction stir forming was first proposed by Nishihara in 2003 [15]. The formation of a macrosize pin from the stirred zone and subsequently forming a rivet interlock is one of the inherent and exclusive phenomena happening in FSF.

A few research groups have conducted the study on the process capabilities and mechanism of joint formation in FSF. The die temperature measurement during cladding of AA6061-T6 over S45C steel sheet by FSF was carried out [16]. Maximum temperature up to 740 K was recorded at 705 rpm and traverse speed of 150 mm/min. It was found that surface temperatures of the die increase with increasing tool rotational speed and tool plunge depth. FSF joints between dissimilar metals like zinc-coated mild steel sheet and aluminum alloys namely, AISI 5182 and AA6014, were also fabricated [17]. In addition to the formation of a perfect mechanical pin interlocking, braze welding was also formed by the diffusion of zinc from the mild steel coating to upper aluminum alloy sheet. The significance of geometrical characteristics such as sheet thickness, pre-drilled hole diameter, and anvil cavity geometry on the joint formation were revealed. Multi-pin configuration and tapered holes possessed better extensibility and toughness. The effect of tool plunge depth, tool diameter, and anvil cavity depth on FSF joints in aluminum to steel sheets was also conducted [18]. It was reported that even at higher tool plunge depths, anvil cavity filling was not complete and unfilled space along with voids were visible on the extruded metal. Modifications on anvil cavity geometry revealed that direction and amount of work material deformation under the tool varies from center to the periphery of the tool. FSF was also utilized for fabricating tungsten embedded copper (C1100) composite having joint strength of 130 MPa, using traversing stir tool rotating at 1200 rpm, 0.05 mm tool plunge, and traverse speed of 100 mm/min [19]. The joint strength was purely contributed by mechanical interlocking with no intermetallic formation. It was also revealed that tool rotational speed and tool tilt angle have a significant impact on heat input, directional heating, and efficient stirring. However, FSF applied on dissimilar alloy combination of same metal has not been studied yet.

FSF shares the same principles of Friction Stir Spot Welding (FSSW) process. Even though FSSW process is efficient in creating spot joints, the characteristic key hole left by the stir tool reduces the mechanical strength of the joint considerably. The thin metal zone generating due to the hook formation in the stir zone is another reason for strength reduction in FSSW. The stir mixing of dissimilar materials also results in intermetallic formation. These drawbacks are eliminated in an FSF process, where the use of a pinless tool prevents the keyhole formation. There is no hook formation in the stir zone of FSF process. Stirring in FSF process is mainly intended to plasticize and extrude the upper sheet metal through the pre-drilled hole in the lower sheet and the stir mixing of upper and lower sheet metals is completely absent. Therefore, the chance of intermetallic formation, which may

deteriorate the joint strength, is less. Unlike FSW and FSSW, it is not appropriate to provide dwell time for FSF as dwell time provides excess heat flux which leads to the severe deformation of the predrilled hole in the lower sheet.

The use of a friction stir tool to obtain mechanical interlocking is an entirely modern concept. However, the exact process analysis and the effect of critical process parameters on the quality of the joint are not yet elaborately studied. In addition, the comprehensive study on the characteristics and mechanical performance of the FSF joints is scarce in literature. The viability of the process for attaining joints in dissimilar grades of same metal is still to be explored. Unlike other joining processes, in FSF, joining such similar materials is more difficult than that of dissimilar metal joining, since the chance of deformation of the lower sheet is more under the frictional heat flux. Lower sheet also gets plastically deformed by the time upper sheet attains enough temperature for forging.

In FSF, it is essential to understand the effect of process parameters such as tool rotational speed, plunge depth and tool features on the joint quality characteristics. Hence, the objective of the present work is to conduct a comprehensive study on the effect of tool rotational speed on the joints formed by FSF process, with a goal of attaining optimized joint strength and conducting joint characterization with the help of mechanical performance studies. The joints formed by FSF have been characterized by examining joint morphology, hardness distribution and macrostructural evolution. Lap shear test, cross-tension test, peel test and tensile test were conducted to quantify the mechanical performance of the joints. Defect formation and failure modes are also presented.

2 Methodology

2.1 Principle

The principle behind FSF process is that a rotating tool heats the upper sheet to a plasticized condition by virtue of frictional contact, followed by forging and extruding the plasticized metal through a prefabricated hole in the lower sheet into an anvil cavity. In this process, plunging of the rotating stir tool onto the surface of the upper sheet generates frictional heat, thereby reducing the flow strength of the upper sheet metal. The heated upper sheet metal is extruded through the predrilled hole provided on the lower sheet which creates the neck of the joint. The deformed metal finally creates a mechanical pin interlock by acquiring the shape of the cavity feature provided on the upper surface of the anvil block. Retraction of the rotating tool at this stage completes the joint formation. Thus, a lap joint formation started by stir heating is finished by the formation of a mechanical pin interlocking. Here, the pin interlock acts like a mechanical rivet. The complete process sequence is schematically illustrated in Fig. 1.

The anvil cavity feature determines the shape of the pin head while extruding the plasticized metal. The diameter of the head formed should be greater than the diameter of the predrilled hole to ensure proper mechanical interlock. If the diameter of the head is nearly equal to that of the pre-drilled hole, the head formed can be easily pulled out through the hole resulting in a weak mechanical interlocking. If the anvil cavity size is increased to form a large pin head, chances are there for the lower sheet to collapse into the anvil cavity while forging. A proper design of stir tool is such that it should generate sufficient and required frictional heat to plasticize upper strip material to facilitate its easier flow into the anvil cavity through the pre-drilled hole. The formation of neck and pin head which determine the joint strength is solely dependent on the work piece material, tool, anvil designs and the process parameters like tool rotational speed and tool plunge depth.

2.2 FSF experiments

The FSF experiments were conducted on an indigenous fixture set up fabricated and mounted on a milling machine (Kirloskar Viking KTM 40) having a wide rotational speed range from 45 to 3500 rpm. The fixture set up fabricated on a

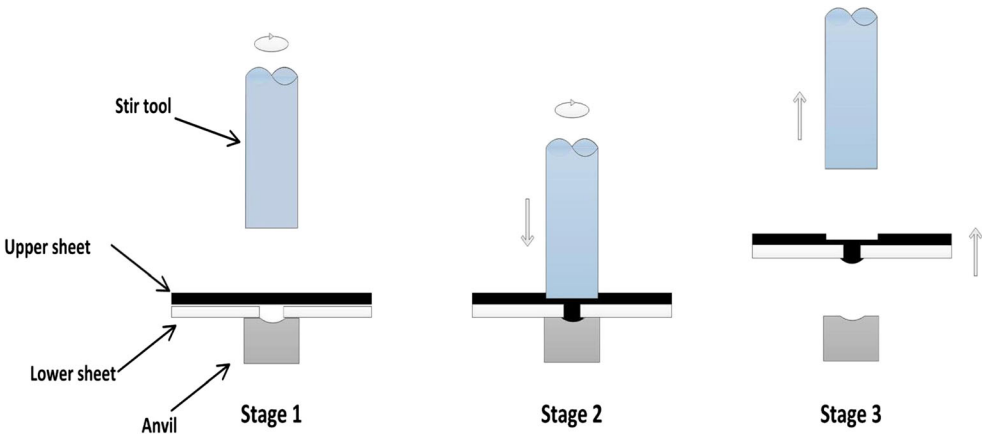

Fig. 1 Stages of friction stir forming (not to scale)

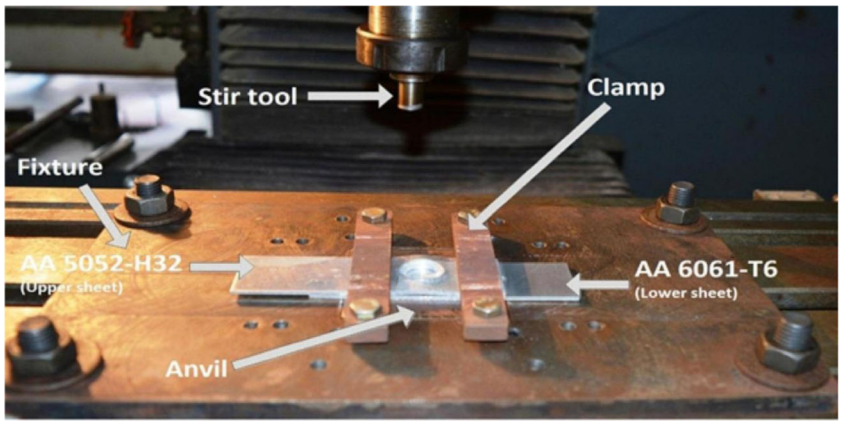

Fig. 2 FSF experimental set-up

mild steel plate was capable of clamping samples of various dimensions for the abovementioned mechanical tests. The fixture had a provision for holding square blocks of anvil at its diagonal center. The top surface of anvil was machined with a hemispherical cavity by spark EDM process. The basic elements of the experimental set up such as friction stir tool, fixture, anvil, and clamps are shown in Fig. 2. The details about anvil and stir tool are given in Table 1.

AA 5052-H32 and AA 6061-T6 sheets are used for the experiments. AA 5052-H32 which forms the upper sheet was stir-heated and form joined into the lower sheet of AA 6061-T6. Each sheet is of 2 mm thickness. The chemical composition of the alloys was obtained through EDX analysis on Zeiss Sigma 002-B Field emission scanning electron microscope, and mechanical properties were obtained through standard tensile test and hardness measurement. The chemical composition and measured mechanical properties of these alloys are given in Tables 2 and 3, respectively. The mechanical properties of the sheet metals were evaluated along the rolling direction of the sheet by following standard procedures.

The metal strips for lap shear, cross-tension, peel, and tensile test were shear cut from large sheets such that the sheet rolling direction is oriented along the length of the samples. The sample dimensions are shown in Fig. 3. A hole of 3 mm diameter was pre-drilled into the lower AA 6061 strip to enable the plasticized upper sheet metal to flow into the anvil cavity during FSF. The proper alignment of stir tool center, pre-drilled hole center on lower sheet, and anvil cavity center along a straight line is important for the formation of a sound FSF joint. The axis of an FSF joint can be considered to be perpendicular to the plane of the sheets passing through the center of the stir spot.

The joints were prepared by varying the tool rotational speed from 500 to 3000 rpm at increments of 500 to obtain the effect of tool rotational speed on the mechanical performance of FSF joints. FSF samples fabricated at lower (500, 1000), medium (1500, 2000), and higher (2500, 3000) rpms were subjected to various mechanical tests and joint cross-sectional studies.

Throughout the experiments, the plunge rate, plunge depth, and direction of tool rotation were kept constant at 0.002 mm/s, 1.5 mm and clockwise direction respectively. Dwell time is not used. Two FSF samples were prepared for each tool rotational speed to ensure the repeatability of the tests. It took nearly 13 min to form an FSF joint. The joint strength tests were carried out on a 100 kN Instron-Dynamic Universal Testing Machine (Model: 8801J4051) where the extension rate was kept constant at 1 mm/min for all the tests.

Table 1 Details of the anvil and FSF tool

Anvil	Material	Mild steel
	Feature	Hemispherical cavity on top surface center
	Cavity diameter	3.5 mm
	Cavity depth	0.55 mm
Tool	Material	H13 tool steel
	Feature	Pinless
	Shoulder diameter	14 mm
	Shoulder length	25 mm

2.3 Mechanical tests

Lap shear test is commonly used for evaluating the shear strength of a lap joint where tensile shear load is applied perpendicular to the axis of the FSF joint. Samples were loaded in the grippers of Instron machine with doublers at the grippers in such a way that the tensile load was applied parallel to its length direction. It was ensured that all lap shear samples failed at the joint location only.

Cross-tension test is commonly used for evaluating the bond strength of a lap joint, where tensile load is applied parallel to the axis of the joint. The upper and lower sheets were aligned to a cross overlapping at the mid-section and joined at its center by FSF process. The samples were loaded in the grippers of Instron machine using custom made fixtures.

Table 2 Chemical composition of the base materials (in % wt.)

Materials	Si	Fe	Cu	Mn	Mg	Cr	Zn	Ti	Al
AA 5052-H32	≤ 0.2	0.1–0.3	≤ 0.2	0.1–0.2	2.8–4.2	0.2–0.3	≤ 0.3	–	Remaining
AA 6061-T6	0.6–0.9	0.2–0.4	0.2–0.3	≤ 0.1	1.4–1.8	0.1–0.4	≤ 0.2	≤ 0.15	Remaining

Peel test is mainly intended to determine the joint strength when the FSF sample is subjected to peeling off operation by pulling the two sheets apart by applying tensile load. The upper and lower sheets were aligned to full overlap and joined at its center by FSF process. The ends of the samples were later bent manually, without affecting the joint, to create space for clamping in the grippers of the testing machine. The samples were loaded in the grippers of Instron machine in such a way that the tensile load was applied parallel to the FSF joint axis.

The above tests were intended to determine the strength of the joint under various loading conditions. The tensile test on FSF samples is performed to evaluate the formability of the joint under uniaxial tensile loading condition. A tensile specimen with FSF joint at the center of the gauge region was subjected to tensile loading. Unlike abovementioned strength tests, where the sheet transfers the load to the FSF joint location, in tensile test, the load is simultaneously shared between the FSF joint and the adjoining sheets of the gauge length region, which enables formability of the FSF joint along with extension of the sheets under uniaxial tensile load. The upper (AA 5052-H32) and lower sheets (AA 6061-T6) were initially wire cut to tensile specimens. The cut specimens were overlapped to a single sample and joined at its center by FSF process. The test specimens were aligned with the center line of the grippers of the testing machine to ensure that only axial tensile stress is developed within the gauge length, without any bending stresses.

In all the mechanical tests, the load-progression data, load at failure, extension at failure were recorded. The failure modes were also observed and analyzed.

Table 3 Mechanical properties of the base materials (along 0° rolling direction)

Mechanical properties	AA 6061-T6	AA 5052-H32
Tensile yield strength (MPa)	225.45 ± 13	155.39 ± 2
Ultimate tensile strength (MPa)	308.40 ± 5	212.705 ± 2
Total elongation (%)	21.44 ± 7	14.82 ± 1
Vickers microhardness (HV)	99.8 ± 6	77.4 ± 9
Strain hardening exponent, n	0.15 ± 0.003	0.161 ± 0.002
Strength coefficient, K (MPa)	489.78 ± 8	355.63 ± 6
Plastic strain ratio, R	0.707	0.589

2.4 Macrostructure, joint morphology, and hardness analyses

The macrostructure analysis of the joint cross-section provides information about the effectiveness of the joint formation, metal flow evolution, defect formation and the distinction of various zones in an FSF joint. The FSF joints were sectioned perpendicular to the length of the sample to reveal the joint cross-section. The cross-section was initially rough finished with emery paper with grit size ranging up to 2000 and fine finish is obtained by polishing with a velvet cloth treated with silvo shine liquid. The polished samples were mild etched with Kellers reagent (190 ml distilled water, 5 mL HNO_3, 3 mL HCl, 2 mL HF) for 20 s. The macrostructure images were taken using Zeiss Axiocam MR3 Microscope at 50× zoom.

Microhardness measurement on FSF samples fabricated at low, medium and high tool rotational speeds were conducted by Vickers indentation method using 500 gf load for 10 s in Buehler MMT3-B Micro Vickers Hardness Tester. Hardness values were taken along the finely polished cross-section of the FSF joints. Array of indentations with 2 mm spacing in between were performed along the joint cross-sections starting from the upper AA5052-H32 strip at one end, through the bonded region up to the other end at a depth of 1 mm from the upper surface (A-Q). Further at the bonded region, one more array of indentation was taken at a 2 mm depth from the upper surface (R-Z) in order to estimate the variation in hardness along the depth of the bonded region. The location of hardness measurements (A-Q and R-Z) is shown in Fig. 4.

Joint morphology analysis refers to the measurement of various structural features developing in an FSF joint and studying the influence of tool rotational speed on its formation. Macrodefects can affect the esthetic appearance of the joint and features like mechanical pin interlock and bond width affects the joint strength. Measurable features include macrodefects such as flash width and flash height of upper and lower sheets (USFW, USFH, LSFW, and LSFH, respectively), upward and sideward bulging of upper sheet (UB and SB), final plunge depth (FPD), joint thickness below the stir spot (SST) and other intrinsic FSF joint features like width and height of mechanical pin (PW and PH) and metallurgical bonding (BW). The joint features are represented over a typical FSF joint cross-section in Figs. 5 and 6. The

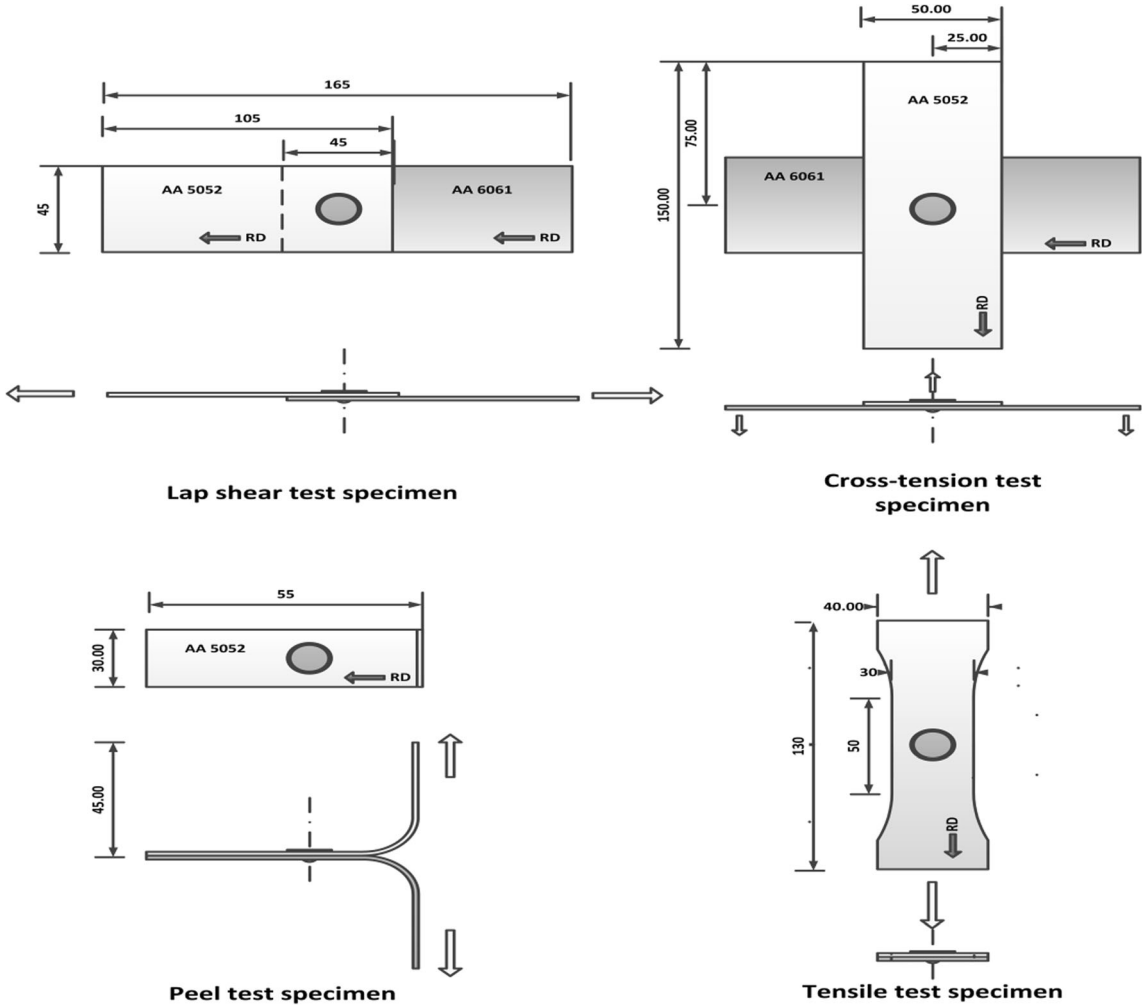

Fig. 3 Dimensions of the test samples for various mechanical tests (all dimensions are in mm, not to scale)

abovementioned geometrical features were measured using a USB digital microscope (DinoliteDinoCapture 2).

3 Results and discussion

In this section, the effect of tool rotational speed on the joint strength and extension at failure through four different mechanical tests, evolution of macrostructure and joint morphology, and modes of failure during testing of the joints are analyzed.

3.1 Performance during lap shear tests

The average fracture load for lap shear samples is plotted against tool rotational speed in Fig. 7a. The fracture load from 500 to 1500 rpms remains almost same at about 6 kN, and it decreases from 1500 to 3000 rpms. A 35% decrease in

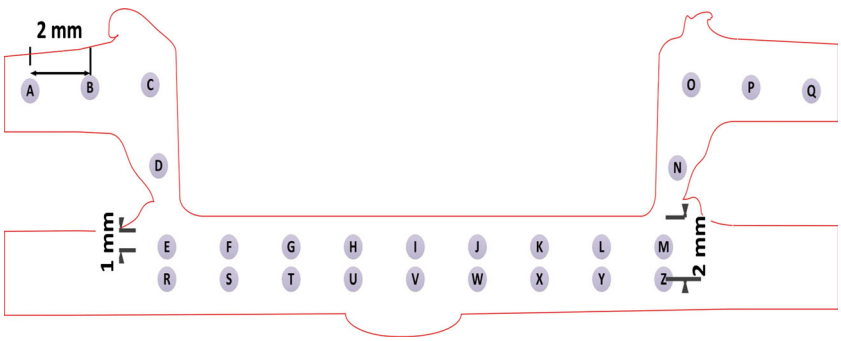

Fig. 4 Location of hardness measurements along the joint cross-section

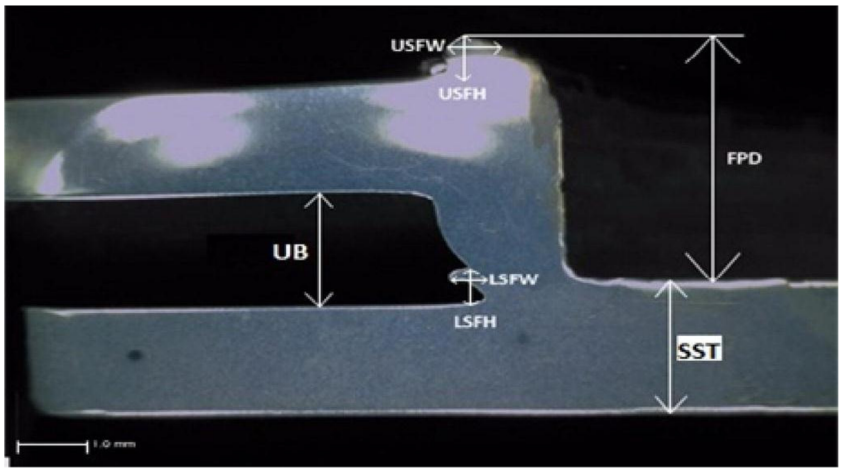

Fig. 5 Morphological features of the FSF joint cross-section (UB—Upward Bulging, LSFW—Lower Sheet Flash Width, LSFH—Lower Sheet Flash Height, USFW—Upper Sheet Flash Width, USFH—Upper Sheet Flash Height, SST—Stir Spot Thickness, FPD—Final Plunge Depth)

fracture load is observed when the tool rotational speed is increased from 500 to 3000 rpm.

The average extension at fracture load for lap shear samples is plotted against the tool rotational speed in Fig. 8a. The extension at fracture load increases from 500 to 1500 rpm. FSF samples for 2000 to 3000 rpms show comparatively low extensibility. A 118% increase in average extension is observed when tool rotational speed is increased from 500 to 1500 rpm. Further a 60% decrease in extension is observed when tool rotational speed is increased from 1500 to 3000 rpm. On the whole, it is found that FSF joints exhibit larger lap shear fracture load and larger extensibility at medium rpm. FSF sample for higher rpm exhibits lower lap shear strength and lower extensibility.

3.2 Performance during cross-tension test

The effect of tool rotational speed on the fracture load during cross-tension test is shown in Fig. 7b. The cross-tension fracture load increases from 500 to 1000 rpm followed by decrease in fracture load up to a minimum at 3000 rpm. A 59% decrease in the cross-tension fracture load is observed when tool rotational speed is increased from 1000 to 3000 rpm.

Figure 8b shows the change in extension at fracture with tool rotational speeds for cross-tension test. The average extension increases from 500 to 1000 rpm and decreases up to 3000 rpm. A 62% decrease in extensibility is observed when tool rotational speed increased from 1000 to 3000 rpm. In summary, FSF sample for higher rpm exhibits lower shear strength and lower extensibility than that at lower and medium rpms.

Similar to lap shear test results, cross-tension samples at high rpms show poor strength and extensibility. The main reason for the variation in strength and extensibility is the influence of frictional heat generation at various tool rotational speeds. From the mechanical tests, it is seen that the extreme heat generation in FSF joint formation at high rotational speeds like 3000 rpm has created a negative impact on both fracture load and extensibility. It is seen that the some of the cross-tension samples showed considerable extension of about 20 mm because of the peculiar nature of the cross-tension test, where the strips of the cross-tension sample undergoes unbending before the tensile load gets concentrated on the spot joint during the test. More details related to this

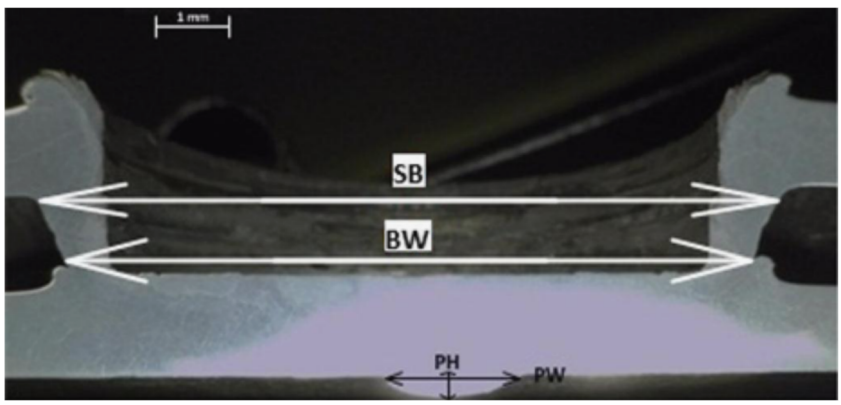

Fig. 6 Morphological features of the FSF joint cross-section (PW—Pin Width, PH—Pin Height, BW—Bond Width, SB—Sideward Bulge)

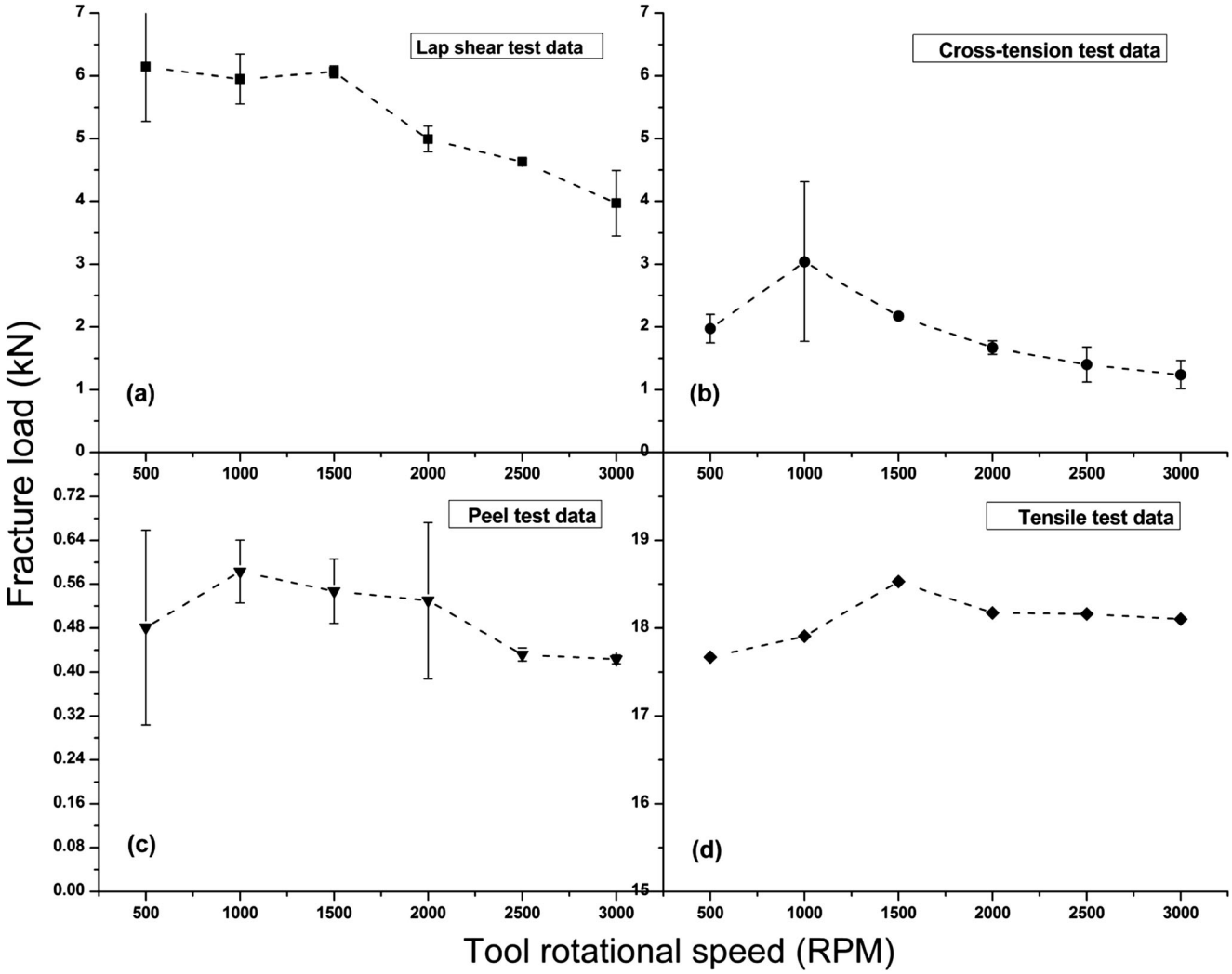

Fig. 7 Comparison of fracture loads at various rotational speeds during mechanical tests

effect are explained with the help of joint macrostructure in Section 3.5.

3.3 Performance during peel test

The fracture load for peel test samples is plotted with respect to tool rotational speeds in Fig. 7c. The peel-off load increases from 500 to 1000 rpm, and then it decreases from 1000 to 3000 rpm. About 27% decrease in the peel-off load is observed, when the tool rotational speed increases from 1000 to 3000. However, the variation in peel-off load is within 1 kN, which is insignificant.

The extension at peel-off is plotted with respect to tool rotational speeds in Fig. 8c. The extension at peel-off increases from 500 to 1500 rpms and then decreases from 1500 to 3000 rpms. The extension at peel-off for FSF samples joined at medium tool rotational speeds (1000, 1500 rpm) are comparatively higher than that for samples joined at high and low tool rotational speeds. About 57% increase in the average extension is observed during peel test when the tool rotational speed increases from 500 to 1500. Further about 49% decrease in average extension is observed when the tool rotational speed increases from 1500 to 3000. FSF sample for high rpm exhibits lower peel strength and lower extensibility. Similar to cross-tension test, some of the peel test samples also showed high extensibility due to bending effect of the strip during the peel test.

It is to be noted that for a sample joined at any particular tool rotational speed, the fracture load is observed to be highest for lap shear sample, lowest for peel test sample and intermediate for cross-tension sample. In general, it can be concluded that average fracture load and average extension at fracture load during above tests are found to be better for FSF samples prepared at low and medium rpms. Therefore, low and medium tool rotational speeds are the best choices for FSF joints between dissimilar grades of aluminum alloys namely AA 5052-H32 and AA 6061-T6 used in the present work. Literature shows

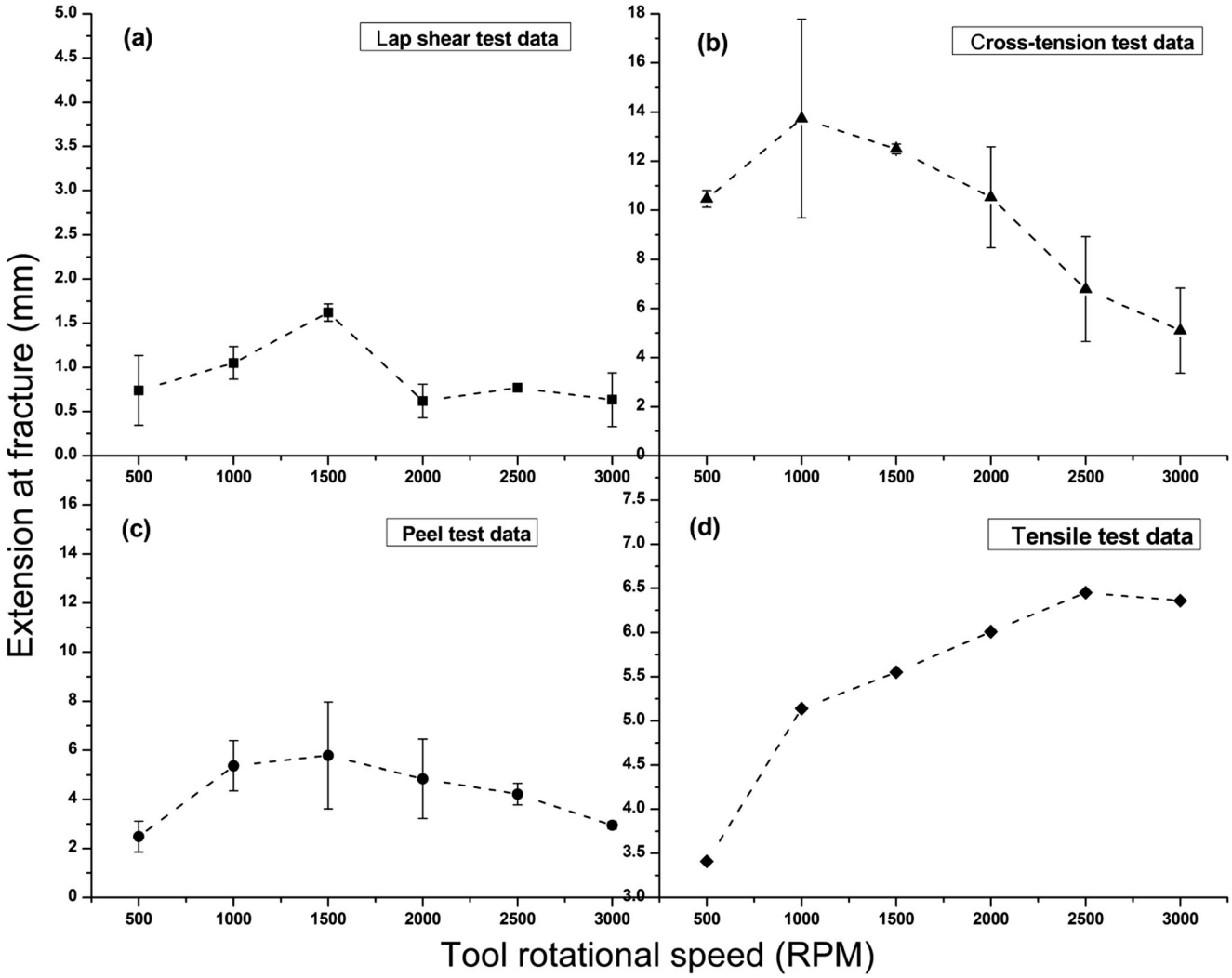

Fig. 8 Comparison of extension at fracture for various rotational speeds during mechanical tests

that the tool rotational speed has a similar effect on FSSW as well. The tensile shear strength of FSSW joints in aluminum alloys, namely 2A12-T4 [20] and 6111-T4 [21], increased up to 1000 and 2250 rpms, and then showed a decreasing trend with increase in tool rotational speed up to 1200 and 3000 rpms, respectively. The lap shear test on FSSW joints between magnesium and aluminum alloys showed that the weld strength decreased with increase in the tool rotational speed [22]. Similar results are also obtained during the present work. Therefore, tool rotational speed has a similar effect on the joint formation in most of the friction-based spot joining processes like FSSW and FSF.

Joining of AA 5052-H32 to AA 6061-T6 with FSW and FSSW was already attempted. Table 4 shows a comparison of joint strength of these joints with FSF joints of the present work. It is observed that FSF joints possess superior joint strength over FSW and FSSW.

Table 4 Comparison of joint strength of FSF with other joining technologies

Joining technique	Joint form	Test type	Maximum load	Reference
Friction stir welding	Butt joint	Tensile test	5.75 kN[a]	[23]
Friction stir welding	Butt joint	Tensile test	4.85 kN	[24]
Friction stir welding	Butt joint	Tensile test	5.93 kN[a]	[25]
Friction stir spot welding	Lap joint	Lap shear test	4.85 kN	[26]
Friction stir forming	Lap joint	Lap shear test	6.14 kN	Present work

[a] Maximum load is calculated from average UTS given in the reference

3.4 Performance during tensile test

The effect of tool rotational speed on the ultimate tensile load during tensile test is shown in Fig. 7d. The ultimate load remains almost same about 18 kN from 500 to 3000 rpms. This shows that the presence of an FSF joints made at different tool rotational speeds at the center of the sample has little effect on the sample strength during the tensile loading. On the other hand, the extension at ultimate load increases from 500 to 2500 rpm (Fig. 8d). About 89% increase in extension at ultimate load is observed when tool rotational speed is increased from 500 to 2500 rpm. The increase in the extensibility may be due to the possible annealing effect of excessive heat generation at higher tool rotational speed. Heat flux from the stir zone at higher rpm might have conducted to the surrounding areas of the gauge length and the resulting heat treatment effect has brought about some increase in the ductility of the tensile samples. Thus, samples joined with FSF shows better formability throughout the rpm range. Literature shows that the formability of friction stir welded AA 6061-T6 sheets evaluated through limiting dome height tests possess better formability than unwelded sheets [27]. Tensile test results showed that strength and ductility of AA 5052 sheets, joined through recently developed joining technique such as friction-stir vibration welded is greater than that of corresponding FSW samples [28]. Therefore, friction stir based joining techniques have the potential to improve the formability of the joining sheets.

3.5 Joint macrostructure analysis and its relation with the mechanical performance tests

FSF samples fabricated at lower, medium and higher tool rpms namely 500, 1500, and 3000, respectively, are selected for macrostructure analysis. The complete macrostructure of the joint cross-section, with schematic representation of various zones are shown in Fig. 9a–c. In Fig. 9a, b, at 500 and 1500 rpms, plastically deformed metal from the upper sheet filled the pre-drilled hole of the lower sheet and further reached the anvil cavity to form a mechanical interlock. Therefore, the approximate pin formation has contributed considerably to the improvement of strength and extensibility of these samples. From Fig. 9c, it is observed that at 3000 rpm, because of the excessive deformation of the lower sheet due to extreme heat generation, the anvil cavity is completely filled by the deformed lower sheet metal. Therefore, the plasticized metal from the upper sheet failed to reach the anvil cavity. The pre-drilled hole undergone closure before the downward metal flow from upper sheet reaches the anvil cavity. Thus, the extreme heat generation at 3000 rpm results in the damage of the pre-drilled hole on the lower sheet. This is the reason for poor joint strength and extensibility of FSF samples fabricated at high tool rotational speeds in the case of lap shear, cross-tension, and peel test samples.

It is observed that in the present work, the heat generation increases with increase in tool rotational speed, which further affects the joint formation. Literature shows that the heat input and processing temperature, during friction based joining technique like FSSW, can be controlled by decreasing the tool rotational speed and dwell time [29]. It was reported that initial increase and subsequent decrease in tensile shear strength with increase in tool rotational speed was mainly due to difference in the size of the annular bond region and the changes in the joint microstructure during FSSW of automotive steels. Similar observations were also found during FSSW of 6111-T4 aluminum alloy. The temperature profiles revealed that the maximum temperature attained (573 K) was low at lower tool rotational speeds, like 1500 rpm, than that at higher tool rotational speeds, like 3000 rpm (688 K) [21]. Likewise, the amount of frictional heat generated at the stir zone increases with increase in rpm of the stir tool and intense plastic deformation, during FSSW of AA 6061-T6 plates [30]. High frictional heat generation caused reduction in the viscosity of the material right under the tool, which further resulted in slippage rather than stirring. The increase in tool rotational speed led to intense stirring and larger stir zone size, but the residual stress formation at the stirred zone induced a negative impact on the formation of AA 5182 FSSW joints, which resulted in poor joint strength at higher tool rotational speeds [31]. Therefore, increase in temperature with increase in tool rotational speed deteriorates the strength of friction-based spot joining processes like FSSW and FSF.

The influence of tool rotational speeds on the joint macrofeatures is discussed here. The various zones that can be identified in FSF joints are Stir zone (SZ), Thermo-mechanically affected zone (TMAZ) and Plastically deformed metal flow zone (PDZ). Perfect metallurgical bonding is observed at all tool rotational speeds. Therefore, no interfacial gaps are visible at the joined region. At the center of the tool impression where the face of the tool touches the upper sheet, a unique pattern is produced by the stirring of the upper sheet metal. This represents the stir zone (SZ), which is confined to upper sheet only. It has been reported that in FSW, the material mixing patterns and subsequent joint strength are quite different for same material combination, depending upon the position of the stronger base material relative to the advancing side [25]. However, no such issues are there in FSF, since it is free from stir mixing of upper and lower sheet materials.

The “onion ring” pattern commonly seen in FSW and FSSW stir zones is clearly observed in FSF joints also (Fig. 10d). The SZ is symmetrically distributed about the center of the joint and possesses a shallow “U” shape with maximum depth at the center. This shows that direction of flow and the amount of work material deformation under the tool varies from center to the periphery of the joint. The width of

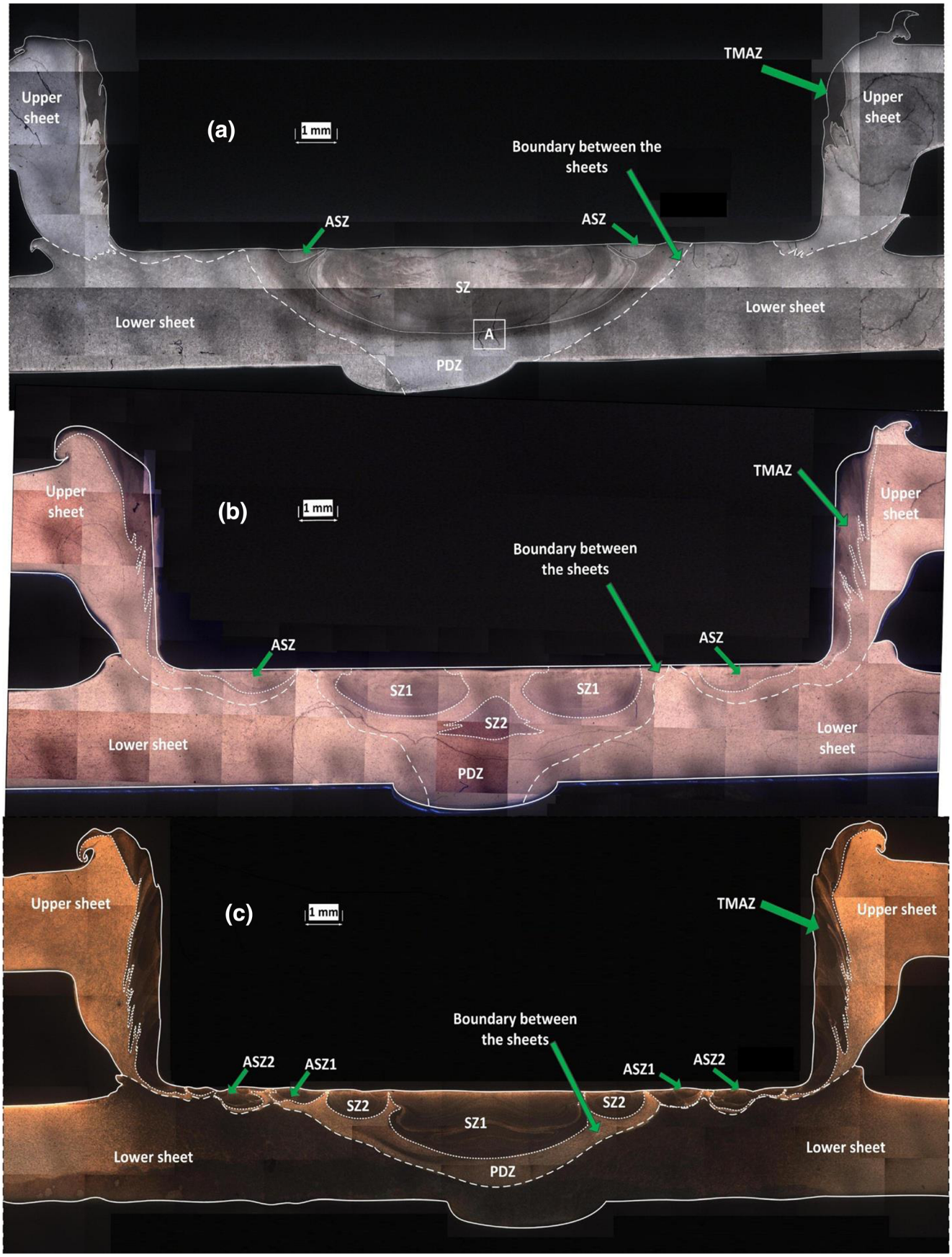

Fig. 9 Joint macrostructure of FSF samples fabricated at **a** 500 rpm, **b** 1500 rpm, and **c** 3000 rpm

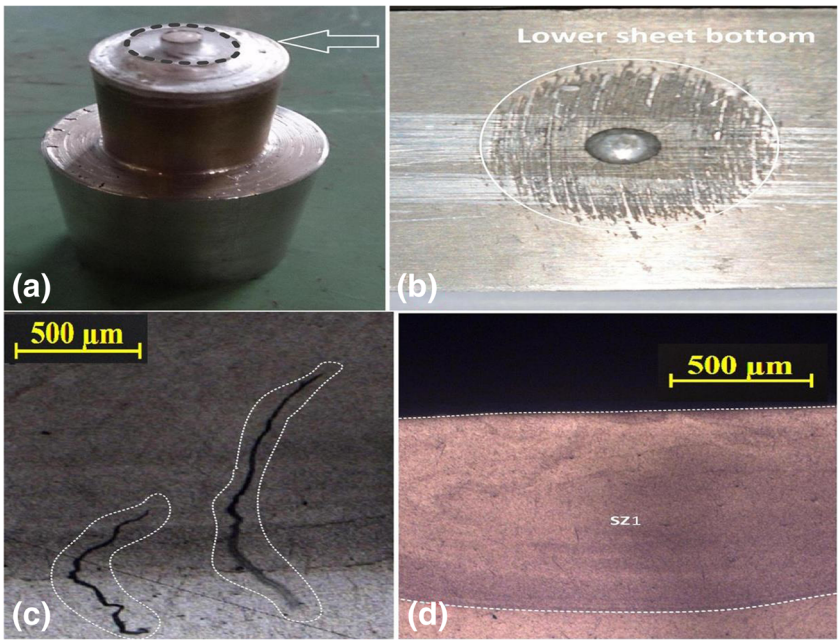

Fig. 10 **a** Stirred upper sheet metal adhered to FSF tool face, **b** surface roughness, **c** cracks over the sample cross-section at location A in Fig. 9a, d "Onion"-like pattern on the SZ1 in Fig. 9b

stir zone increases and partitions within the stir zone are formed with increase in the tool rotational speed as seen from the macroscopic images. At 500 rpm, SZ is unique and no partitions in SZ are visible. At 1500 rpm, SZ is localized and clear separation between the stir zones is visible. At this tool rotational speed, two distinct stir zones SZ1 and SZ2 are visible. SZ1 is visible near the upper sheet surface and SZ2 is visible just below SZ1, at the center, fully enclosed. At 3000 rpm, localized SZs are distributed over the joint cross-section.

Raj Kumar et al. [24] reported that cylindrical threaded pin rendered excellent bondage due to effective stirring and mixing, during FSW of AA5052-AA 6061 aluminum alloys for which a tensile strength of 4.85 kN was obtained. The FSF joints in the present work, on the same material combination, shows a lap shear strength of 6.14 kN wherein stir mixing of upper and lower sheets is absent. Therefore, stir mixing seen in FSW and FSSW is not only the primary factor for contributing excellent strength for friction-based joints in aluminum alloys but also factors like metallurgical bonding and mechanical interlocking as seen in FSF that play significant roles.

Plastically deformed metal flow zone (PDZ) is located just below the stir zone, where the stirring of the plasticized metal is absent. Here, the metal is forged, and metal flow occurs radially inward into the anvil cavity through the pre-drilled hole due to compressive pressure generated by the downward movement of the stir tool. As seen in Fig. 9c, at 3000 rpm, the SZ and the PDZ are clearly distinguished.

The schematic representation of metal flow directions over the joint cross-section of 500, 1500, and 3000 rpm FSF samples is shown in Fig. 11a–c. It can be observed that since the stir tool is pinless, the SZ metal just beneath the center point of the stir tool never undergoes stirring due to the zero torque and instead it flows in the downward direction through the partitions of the SZ during the downward tool plunge. The downward flow not only enhances the pin formation but also affects the deformation of the heated lower sheet. The downward flow is prominent only at lower and medium rpms like 500 and 1500 but absent at 3000 rpm.

The TMAZ is visible on the side walls of the tool impression (Fig. 9). The frictional contact of lateral surface of the tool over the side walls and high angular momentum of the tool contribute the formation of TMAZ. The TMAZ seems to have moved upwards near the side walls, as shown in samples fabricated at medium and high tool rotational speeds, due to intense tool plunge force combined with high tool rotational speeds. The width of the TMAZ increases with increase in the tool rotational speed (Fig. 9a–c). At medium and higher rpms, the TMAZ generated on the side walls of the joint become prominent, which in turn contributes to the heat generation (Fig. 9b, c).

Annular stir zone (ASZ) is a feature exclusively observed in the macrostructure of FSF joint cross-sections. These are ring-shaped stir zones surrounding the main SZ observed in the cross-sections of FSF samples fabricated at medium and higher tool rotational speeds. These are completely isolated from central SZ and are visible as symmetrical stir zone islands located on both sides of the central SZ in the FSF cross-section. The main reasons for the formation of these ASZs are the outward radial flow of hot plasticized upper metal due to the downward tool plunge force and the upward distortion of the lower sheet under the influence of heat flux from the SZ. The upper sheet possesses both inward and outward radial flow during the tool plunge, which reduces the

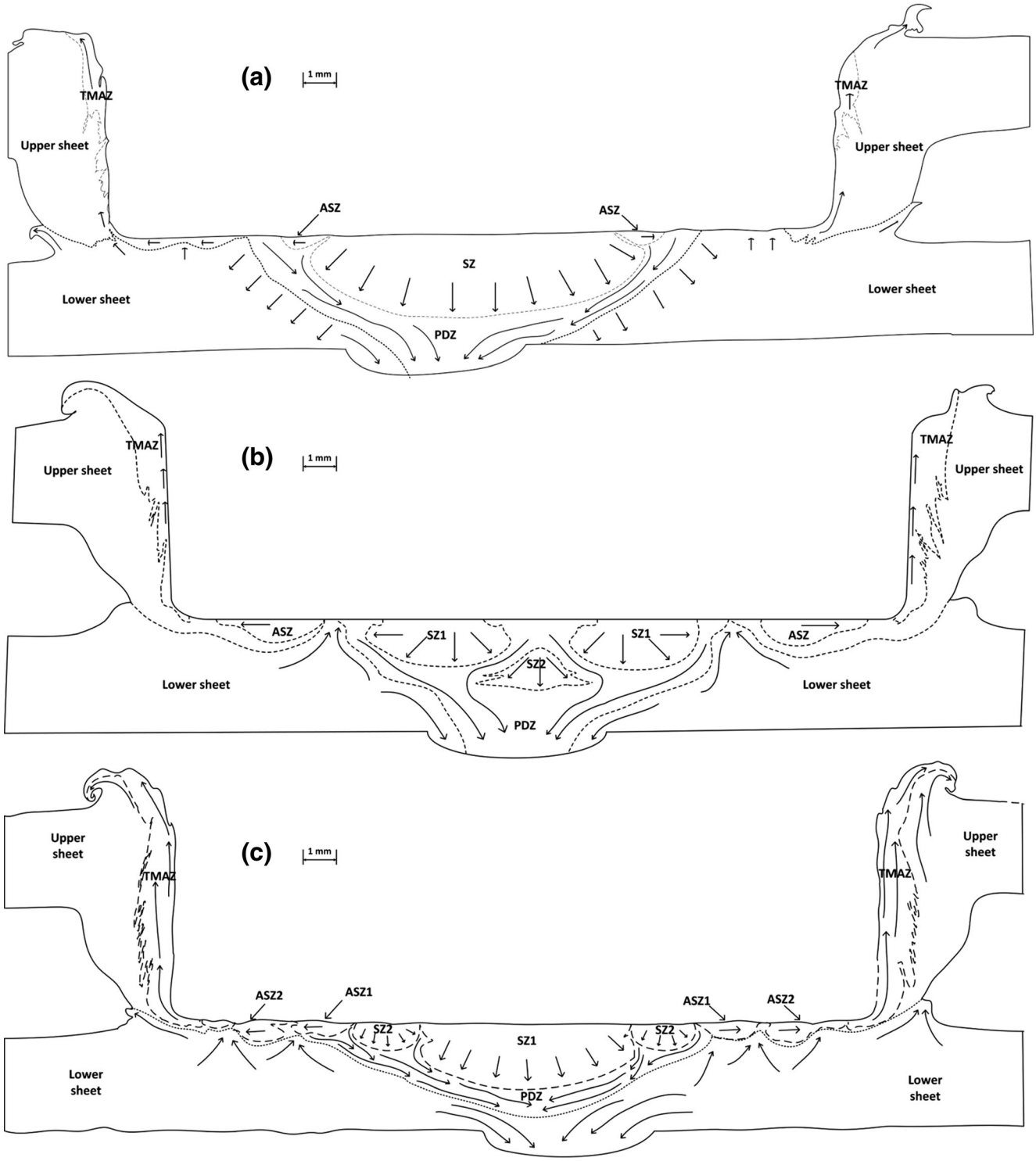

Fig. 11 Schematic representations of the FSF joint cross-section at **a** 500 rpm, **b** 1500 rpm, and **c** 3000 rpm with metal flow directions indicated

thickness of the upper sheet metal beneath the face of the tool. Inward radial flow of the hot plasticized metal beneath the SZ promotes the pin formation. Meanwhile, the outward radial flow of the upper sheet metal due to the high tool plunge force increases the width of the SZ and the upward distortion of the lower sheet promotes the formation of annular stir zone from the main SZ. The ASZ visible at 500 rpm is small sized and found attached to the central SZ. At 1500 rpm, ASZ is completely isolated from the central SZ, and at 3000 rpm numerous ASZs are visible.

The macrostructure analysis shows that at high tool rotational speeds, exact rivet-like pin formation from the upper

sheet stirred metal is not practical. The extreme compressive pressure developed by the downward tool plunge resulted in considerable deformation of the lower sheet. Further, the heat flux from the plasticized SZ accelerated the deformation of the lower sheet. In addition, the closure of the pre-drilled hole hindered the smooth extrusion of plasticized metal from the upper sheet at higher rpm; thereby mechanical pin interlocking is poorly developed. FSF joint formation is complete only when there is mechanical pin interlocking and metallurgical bonding. At high tool rotational speeds, only metallurgical bonding has been generated, but mechanical interlocking is missing. Thus, it can be inferred that high tool rotational speeds like 3000 rpm are not favorable for FSF joints in similar metal combinations. This is particular only with FSF joint formation in similar sheet metal combination, for which high heat flux has a negative impact on the joint formation. However, the joints made at 3000 rpm also possess a sound joint appearance even though the required forging of plasticized upper sheet metal through the predrilled hole in the lower sheet is absent.

FSF joining trials at 500 rpm failed at certain attempts due to upper sheet failure like sticking of plasticized stirred metal on the face of the pin-less tool as shown in Fig. 10a. This is due to higher sticking friction at the tool-upper sheet interface at lower tool rotational speeds. Excessive tool vibration was observed for FSF samples fabricated at 3000 rpm. This may be attributed to the slippage at the tool-upper sheet interface at higher tool rotational speeds. These vibrations might have influenced the damage of the pre-drilled hole and the poor mechanical performance of FSF joints at high tool rotational speeds. No cracks are visible at the outer surface of the upper sheet metal extruded into the anvil cavity in the FSF joints fabricated during the present work despite such observations were reported, while FSF joints were fabricated between AISI 6014 aluminum alloy and GMW2 mild steel [32].

3.6 Hardness variation

Figure 12 shows the hardness variation along the upper array (locations A to Q in Fig. 4) over the cross-section of the FSF samples fabricated at lower (500 rpm), medium (1500 rpm), and higher (3000 rpm) tool rotational speeds. The hardness of the FSF joints is found to be lesser than that of the parent metals. The inverted "W"-shaped hardness profile typical for a pin tool friction stir process is observed in all FSF samples. Highest hardness is observed at the boundary of the stir zone (locations G and K) where the upward distortion of the lower sheet is observed. For all FSF samples, SZ possesses lower hardness and a decrease in the hardness is observed towards SZ center (location I). This asserts the fact that zero torque at the center of the pin-less tool induces no stirring other than downward plunging of the plasticized metal and subsequently enhances the formation of softer region at the center of the SZ.

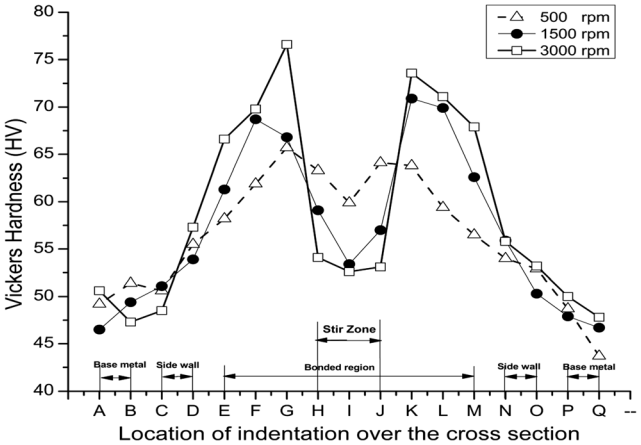

Fig. 12 Comparison of hardness variation along the joint cross-section fabricated at various tool rotational speeds

An increase in torque in the radial direction of the pin-less tool induces considerable stirring and subsequent formation of stronger region towards the SZ periphery (locations H and J).

Beyond the stir zone, hardness values decrease towards the outer periphery of the cross-section of FSF samples (locations F to A and L to Q). A decrease in the hardness of about 25 HV than the parent metal hardness is observed at the base metal of the cross-section. This shows that considerable heat flux conducted from the SZ has induced some heating effect on the surrounding region of the FSF joint.

It is observed that hardness of the SZ decreases with increase in the tool rotational speed. Maximum and minimum hardness at the SZ is observed for FSF sample fabricated at 500 and 3000 rpm, respectively. With increase in the tool rotational speed, the hardness variation between locations G and H, J and K increases. Maximum variation in the hardness is observed for FSF sample fabricated at 3000 rpm and minimum for FSF sample at 500 rpm. This shows that increase in the tool rotational speed has induced considerable stirring and subsequent formation of harder regions at the boundary of the SZ.

The comparison of the hardness over the depth of the cross-section (locations E to M and R to Z of Fig. 5) of FSF sample fabricated at 1500 rpm is shown in Fig. 13. An inverted "W"-shaped hardness profile is also observed along the lower array of indentations. The hardness measurements are coinciding at locations over the extruded pin namely I and V. Since AA 6061-T6 is harder than AA 5052-H32, lower array of indentation possesses hardness values greater than or equal to that of upper array of indentation. Increase in the hardness over the depth of cross-section is also contributed by the compressive deformation of lower sheet under the extreme tool plunge force, though the variation is insignificant.

3.7 Joint morphology analysis

The comparison of morphological features (refer to Figs. 5 and 6) in the FSF joint cross-section is shown in Table 5. It

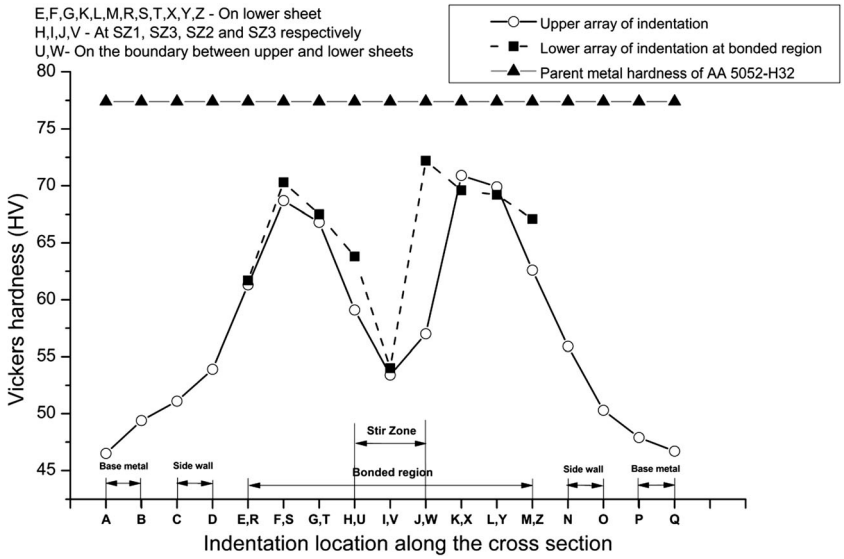

Fig. 13 Hardness variation along the depth of the joint cross-section of FSF sample fabricated at 1500 rpm

is observed that pin width (PW), pin height (PH) and bond width (BW) which determine the joint strength, remain almost same for FSF joints when tool rotational speed is varied from 500 to 3000. Stable pin width and pin height ensures that the anvil cavity filling during pin formation is perfect irrespective of the variation in tool rotational speed. This shows that tool rotational speed does not have any influence on those external geometric features influencing the strength of the FSF joint.

Upward bulging of the upper sheet (UB) is a distortion defect seen in FSF due to the constraining effect of fixture clamps that restrict the thermal expansion of upper sheet in length direction of the sample. The stirring and axial force might have resulted in excessive upward protrusion of stirred metal along the lateral surface of the tool, which resulted in considerable upward bulging of the upper sheet. UB is minimum in case of 1500 rpm, about 2.13 mm, and maximum in case of 2500 rpm, about 2.65 mm, and at all other tool rotational speeds, UB varies in between. So the change in UB is insignificant w.r.t the tool rotational speed. The reason may be that the constant tool plunge depth of 1.5 mm induced almost similar upward bulging of upper sheet throughout the range of tool rotational speeds. In addition to UB, sideward bulging (SB) of upper sheet is also observed for all samples. Maximum and minimum sideward bulge diameter of 18.11 and 17.52 mm is recorded for FSF samples fabricated at 2500 and 1000 rpms, respectively. Since the upper sheet can freely bulge in upward and sideward directions within the clamped region, most of the samples show random measurements in bulge values and a trend has not observed with change in tool rotational speeds.

Plunge depth (FPD) of the tool creates stir spot on the surface of the upper sheet. Like UB, measured values of the plunge depth also remains constant with increase in the tool rotational speed. This is because the upper sheet bulging consequently affects the depth of tool impression on the FSF spot joint.

Flash is generally a deformation occurs in upper and lower sheets, where the material is free to bulge out in any direction (USFW, USFH, LSFW, LSFH). The comparison of these measurements at various tool rotational speeds

Table 5 Measured values of the morphological features on FSF joint cross-section

Tool rotational speed (rpm)	PW (mm)	PH (mm)	BW (mm)	UB (mm)	SB (mm)	FPD (mm)	USFW (mm)	USFH (mm)	LSFW (mm)	LSFH (mm)	SST (mm)
500	3.55	0.56	16.47	2.16 ± 0.06	17.85	4.51 ± 0.13	1.68 ± 0.17	0.79 ± 0.01	0.58 ± 0.04	0.81 ± 0.014	2.39 ± 0.14
1000	3.34	0.52	16.0	2.28 ± 0.13	18.11	5.21 ± 0.011	1.84 ± 0.24	0.89 ± 0	0.50 ± 0.01	0.74 ± 0	2.39 ± 0.10
1500	3.58	0.53	16.2	2.13 ± 0.11	17.98	4.62 ± 0.11	1.26 ± 0.05	0.77 ± 0.06	0.44 ± 0.04	0.79 ± 0	2.23 ± 0.06
2000	3.19	0.48	16.29	2.37 ± 0.19	17.67	5.10 ± 0.03	1.48 ± 0.2	0.78 ± 0.09	0.52 ± 0.05	0.83 ± 0.043	2.47 ± 0.14
2500	3.55	0.52	16.12	2.65 ± 0.25	17.52	5.63 ± 0.11	1.70 ± 0.12	0.71 ± 0.03	0.35 ± 0	0.50 ± 0.0385	2 ± 0.09
3000	3.35	0.51	16.29	2.41 ± 0.08	17.82	5.01 ± 0	1.43 ± 0.13	0.75 ± 0.01	0.21 ± 0.03	0.60 ± 0.0335	2.21 ± 0.09

(PW—Pin Width, PH—Pin Height, BW—Bond Width, UB—Upward bulging, SB—Sideward Bulging, FPD—Final Plunge Depth, USFW—Upper Sheet Flash Width, USFH—Upper Sheet Flash Height, LSFW—Lower Sheet Flash Width, LSFH—Lower Sheet Flash Height, and SST—Stir Spot Thickness)

shows that flash formation is random in nature and the width and height of the flash are not varying much w.r.t tool rotational speed.

Stir spot thickness (SST) of FSF joints fabricated at various tool rotational speeds is also given in Table 5. The actual SST is found to be in the range of 2 to 2.39 mm, when 2.5 mm was the expected SST. The difference between the actual and the expected SSTs is negligible. Thus, measured values of abovementioned morphological features show that their variation is negligible and they are independent of the tool rotational speed during FSF joint formation.

3.8 Miscellaneous joint features

The following are the miscellaneous features generated during the FSF of AA 5052-H32 and AA 6061-T6 sheets as observed from the present work.

(i) A small misalignment between stir tool center and anvil cavity center is visible on the macrostructure of the 500 rpm FSF sample (Fig. 9a), where the pin formation is affected by the slight eccentricity of the anvil cavity towards the periphery of the stir tool center. However, the strength of the joint is not impaired much.

(ii) Cracks are visible throughout the cross-section of FSF samples fabricated at low and medium tool rotational speeds, even at the stir mix zone, which might be generated due shrinkage of the hot plasticized metal during cooling (Fig. 10c).

(iii) Flash is an undesirable defect that occurs over the upper and lower sheet as a protrusion around the circumference of the stir spot created by the FSF stir tool. Flash seems to have little effect on the joint strength since the formation of the mechanical pin interlocking and metallurgical bonding is complete in all joints irrespective of the size of the flash. However, flash possesses some safety concerns and affects the esthetic appearance of the joint. The reason behind the formation of lower sheet flash is that the high plunge depth value of 1.5 mm on a 2 mm upper sheet have induced some amount of deformation on the lower sheet also, which resulted in the upward bulging of lower sheet, generating flash below the circumference of the stir spot.

(iv) Surface roughness is a another feature generated on the bottom of the lower sheet where it is can be clearly distinguished by the presence of a vivid circular roughness area having same diameter as that of the friction stir tool (Fig. 10b). These rough markings are generated due to extreme mechanical squeezing and thermal effect of the FSF process on the lower sheet.

3.9 Modes of failure during mechanical testing

Tear-off, partial bond delamination, and pull-out are the three failure modes observed for FSF samples in lap shear, cross-tension, and peel tests as shown in Fig. 14.

- In tear-off failure mode, the upper sheet has undergone tearing off over the circumference of the stir spot leaving the complete bonded region stuck on the lower sheet. This mode of failure happens mainly due to the thinning of the upper sheet near the circumference of stir spot irrespective of the pin formation.
- In partial bond delamination failure, the bonded region undergoes partial delamination, finally leaving the extruded pin and some bonded region at the stir spot over the lower sheet. This mode of failure is attributed to the poor metallurgical bonding around the circumference of the stir spot even though proper pin formation is occurred.
- In pull-out failure, the bonded region has undergone complete delamination resulting in the separation of the upper and lower sheets apart. Distorted lower sheet hole is also visible on the samples failed by pull-out mode. Thus poor metallurgical bonding and imperfect pin formation together creates pull-out failure.

The main reason behind the failure modes are the weak zone formation at critical regions of the FSF joint. The two critical regions are (a) the outer circumference of the stir spot in the upper sheet (critical region 1) and (b) the distorted lower sheet which protrudes upwards and separate the central stir zone and the annular stir zones (critical region 2).The thinning of the upper sheet near the circumference of the stir spot is mainly responsible for tear-off failure. The upward distortion of the lower sheet creates weak zone near the surface of the stir spot, which results in partial bond delamination failure. Figure 15 shows the schematic of the critical weak zones in the cross-section of the FSF joint fabricated at 1500 rpm.

Jeon et al. [26] reported that the failure mechanism of AA 5052-AA 6061 FSSW joints under quasi-static shear loads was strongly affected by the stress concentration induced by the hook formation near the SZ. Similarly, failure modes in FSW joints depend on the position of the softer base metal relative to the advancing side [25]. However, the failure of FSF joints initiates from the critical regions as mentioned above. This is the reason for FSF joints showing different modes of failure other than that in FSW and FSSW joints.

Table 6 shows the summary of the failure modes, at various tool rotational speeds from 500 to 3000 rpms, of FSF samples prepared for lap shear, cross-tension, and peel tests. Tear-off failure is the most common failure seen in FSF samples, followed by partial bond delamination. Pull-out failure occurs in very few cases. It should be noted that FSF samples

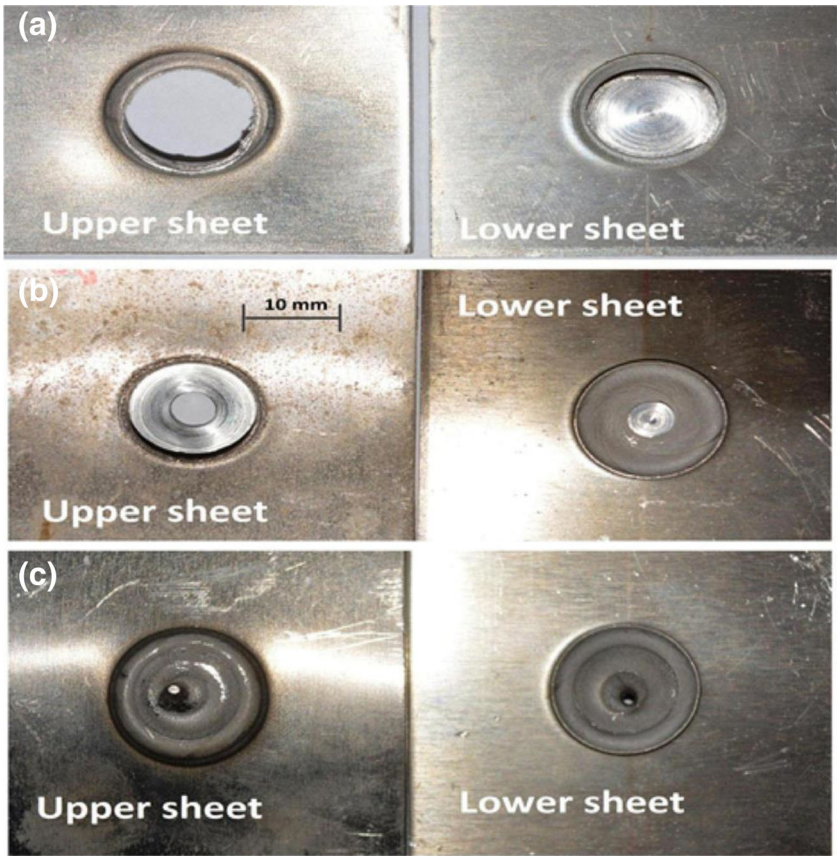

Fig. 14 Modes of failure: **a** tear-off, **b** partial bond delamination, **c** pull-out failure

prepared at 1500 and 3000 rpms showed all the three modes of failure during the mechanical testing, while samples made at other rpms showed any two of the three failure modes. Therefore, the modes of failure are random and have no appropriate relation with tool rotational speed. Moreover, the failure modes are random with respect to the trials at same tool rotational speed for a particular test.

Figure 16 shows the comparison of load-progression behavior during cross-tension test of FSF samples fabricated at 500, 1500, and 3000 rpms for the two different joining trials. From Fig. 16a, at 500 rpm, it can be seen that for partial bond delamination failure, just after the initiation of fracture, the decrease in the load is gradual, till the sample attains full separation between the upper and lower sheets. Therefore, partial bond delamination failure is gradual in nature when compared to tear-off failure although extension acquired after the initiation of fracture remains almost same for both the samples. The gradual failure in partial bond delamination mode is clearly seen in load-progression behavior of FSF sample fabricated at 1500 rpm, as shown in Fig. 16b. Pull-

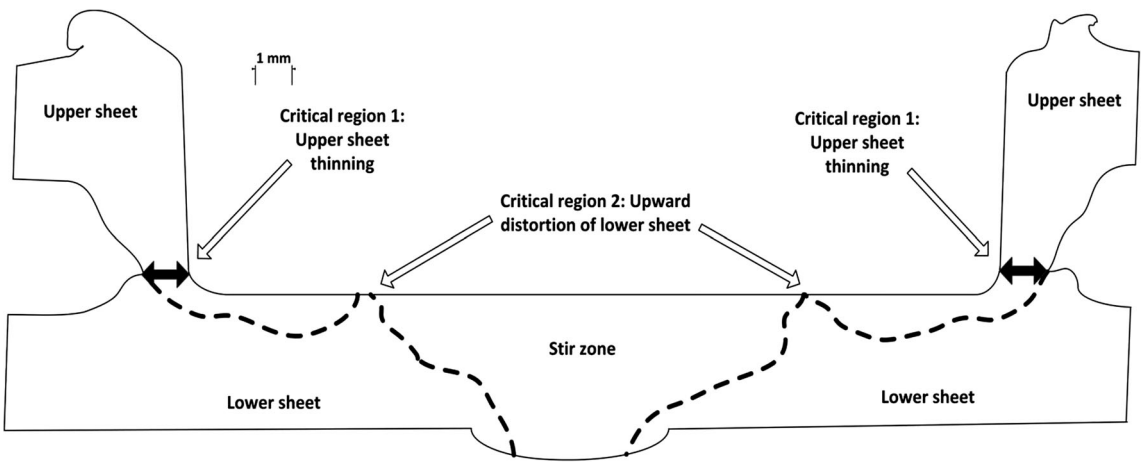

Fig. 15 Weak zone formation over the cross-section of the FSF sample

Table 6 Modes of failure

RPM	Lap shear test		Cross-tension test		Peel test		Tensile test
	Trial 1	Trial 2	Trial 1	Trial 2	Trial 1	Trial 2	
500	Partial bond delamination	Partial bond delamination	Partial bond delamination	Tear-off	Tear-off	Tear-off	Stir spot fracture
1000	Tear-off	Tear-off	Tear-off	Partial bond delamination	Tear-off	Tear-off	Stir spot fracture
1500	Partial bond delamination	Tear-off	Partial bond delamination	Pull-out	Partial bond delamination	Tear-off	Stir spot fracture
2000	Tear-off	Tear-off	Pull-out	Pull-out	Tear-off	Tear-off	Base metal fracture
2500	Tear-off	Tear-off	Partial bond delamination	Partial bond delamination	Partial bond delamination	Tear-off	Base metal fracture
3000	Partial bond delamination	Tear-off	Pull-out	Tear-off	Tear-off	Partial bond delamination	Base metal fracture

out and tear-off failures modes are sudden in nature, which can be seen from the comparison of load-progression behavior of FSF samples fabricated at 3000 rpm, as shown in Fig. 16c.

The tensile test samples show entirely different modes of failure. Some of the samples show base metal fractures, while others show stir spot fracture (Fig. 17a, b, respectively). The

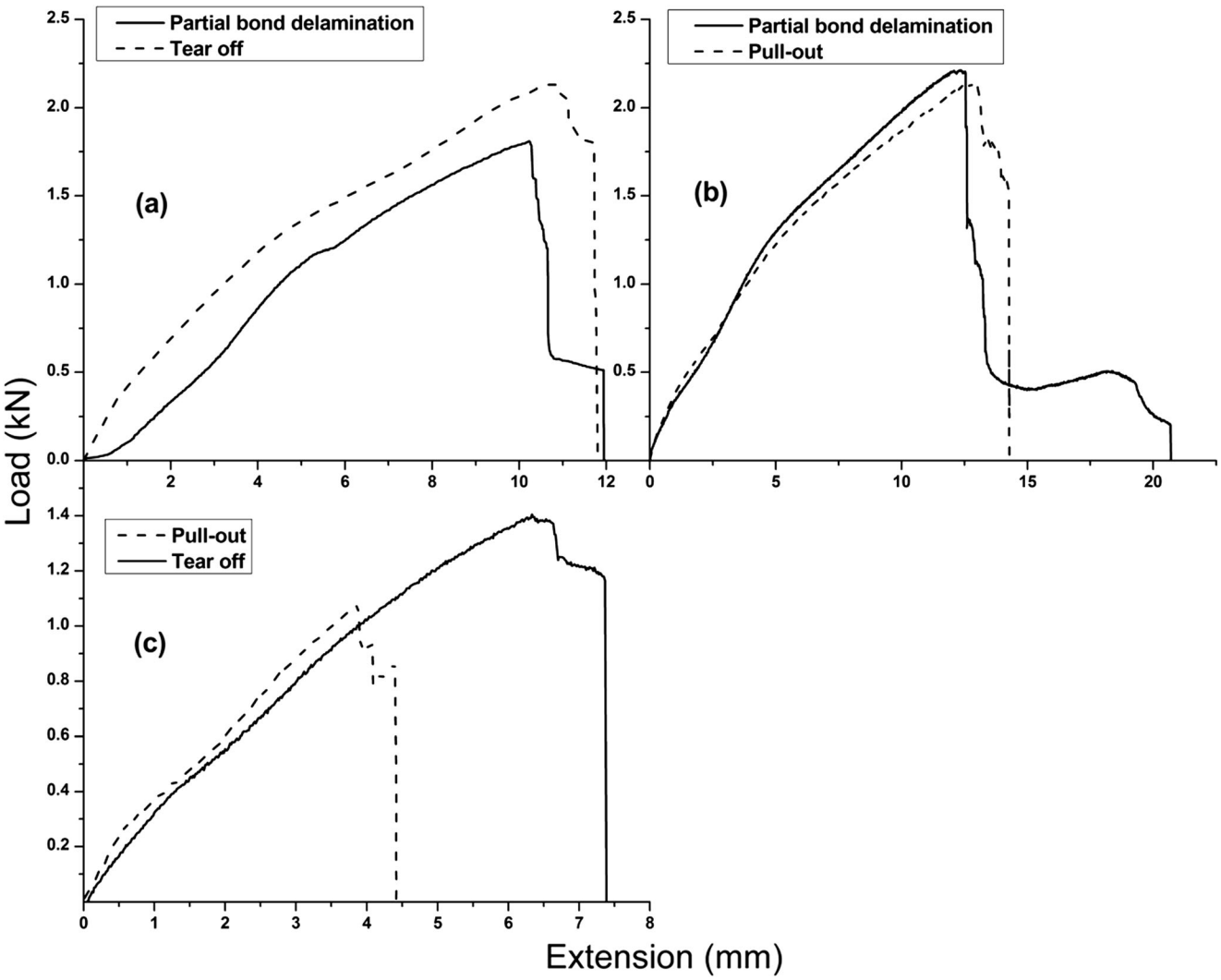

Fig. 16 Load-progression behavior of cross-tension samples at **a** 500 rpm, **b** 1500 rpm, and **c** 3000 rpm

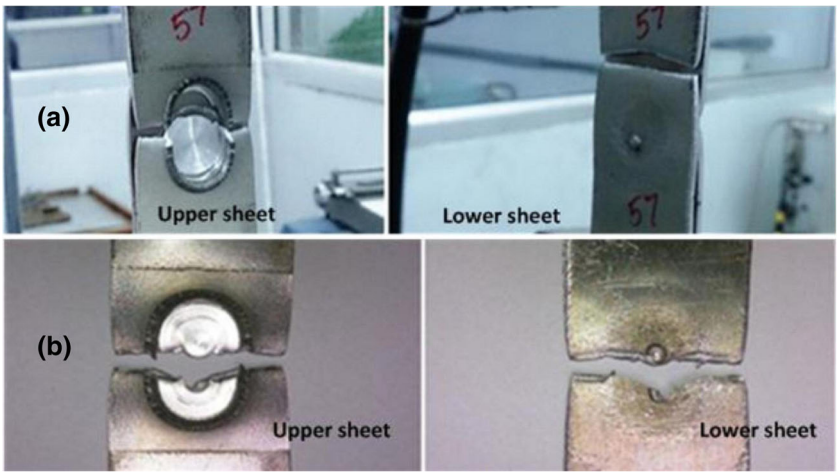

Fig. 17 Modes of failure in tensile test: **a** base metal fracture (500–1500 rpm); **b** stir spot fracture (2000–3000 rpm)

reason behind the occurrence of these failure modes is that the FSF joints have undergone considerable forming before the initiation of failure during the tensile test. Necking commonly seen in uniaxial tensile test is also observed in these FSF samples.

The summary of failure modes during tensile test of FSF samples fabricated at various tool rotational speeds is also shown in Table 6. It is observed that FSF samples at lower rpm show stir spot fracture and those at higher rpm show base metal fracture. Stir spot fracture occurs when the sample has not undergone considerable forming, and ultimately, failure initiates from within the joint. The heat generation at lower rpm may not be excessive to increase the ductility that most of the samples fail at the stir spot, which is the critical geometrical inhomogeneity in the tensile samples. Base metal fracture occurs due to the enhanced ductility of the sheet adjacent to the FSF joint, which has undergone thermal treatment due to the excessive heat flux from the stir spot. Thus, base metal fractures when the strength of the adjacent sheet region is less than the joint strength. FSF samples fabricated at medium tool rotational speeds show both the failure modes.

4 Conclusion

Friction stir form joining of 5052-H32 and AA 6061-T6 is conducted, and the following conclusions are drawn from the results of the present work.

- FSF can be successfully used to join sheet metals of almost same quality, namely AA 5052-H32 and AA 6061-T6, in which obtained lap shear strength of 6.14 kN is far better than that of other friction based joining technologies like FSW and FSSW.
- The mechanical performance studies revealed that the fracture load and extensibility show an increasing trend or nearly same trend, with increase in the tool rotational speed from 500 to 1500 rpm, while a decreasing trend is observed with increase in the tool rotational speed from 1500 to 3000 rpm.
- The main reason for the variation in the joint strength is the influence of increase in frictional heat generation with increasing tool rotational speed. The extreme heat generation at higher tool rotational speeds like 3000 rpm has deteriorated the fracture strength and extensibility of FSF samples. No pin formation was initiated at these RPMs. Therefore, low and medium tool rotational speeds, from 500 to 1500 RPM, are the best choices for fabricating FSF joints between AA5052-H32 and AA 6061-T6 sheets.
- FSF samples subjected to tensile test showed almost similar fracture loads, while an increase in the extensibility is observed with increase in the tool rotational speed due to high heat flux.
- The optical macrostructure analysis of joint cross-sections revealed the presence of four distinct zones on the joint cross-section namely stir zone, thermo-mechanically affected zone, plastically deformed metal flow zone, and annular stir zone. The increase in tool rotational speed has resulted in the formation of partitions within the stir zone and increase in the size of thermo-mechanically affected zone. Upward distortion of the lower sheet due to heat flux from the stir zone results in the formation of annular stir zone.
- It is revealed that the inward radial flow of plasticized metal from the plastically deformed metal flow zone through the pre-drilled hole in the lower sheet results in the mechanical pin formation.
- Inverted "W"-shaped hardness profiles show that the increase in the stirring effect with increase in tool rotational speed produces harder regions towards the SZ boundary. In addition, the hardness of the central stir zone decreases with increase in the heat flux at high tool rotational speeds.
- The joint morphology analysis revealed that the formation of external structural features, which affects the joint

strength and esthetic appearance, is independent of the tool rotational speed.
- Three modes of failure namely partial bond delamination, tear-off, and pull-out are observed during the mechanical performance tests, which are initiated by the critical weak zone formation due to upper sheet thinning, improper bonding, and upward distortion of the lower sheet. The modes of failure are random in nature and they are independent of the tool rotational speed.

It can be concluded that the tool rotational speed has a profound influence on the joint strength of FSF samples. Generally, Al-Steel spot joining with FSF is more simple as the bottom steel sheet will act as a rigid body and hence extrusion of Al alloy into the anvil cavity through pre-drilled hole in the bottom sheet is easier. In this context, joining of dissimilar grade aluminum alloys with FSF, attempted in the present work, is a significant contribution.

Acknowledgements The authors thank the mechanical testing facility extended by the Central Instruments Facility, IIT, Guwahati, for conducting the mechanical performance tests.

References

1. Lee CJ, Lee JM, Ryu HY et al (2014) Design of hole-clinching process for joining of dissimilar materials—Al6061-T4 alloy with DP780 steel, hot-pressed 22MnB5 steel, and carbon fiber reinforced plastic. J Mater Process Technol 214:2169–2178. https://doi.org/10.1016/j.jmatprotec.2014.03.032
2. Thomas W, Nicholas E (1997) Friction stir welding for the transportation industries. Mater Des 18:269–273. https://doi.org/10.1016/S0261-3069(97)00062-9
3. Sathiya P, Aravindan S, Haq AN (2005) Mechanical and metallurgical properties of friction welded AISI 304 austenitic stainless steel. Int J Adv Manuf Technol 26:505–511. https://doi.org/10.1007/s00170-004-2018-6
4. Zhang Z, Zhang HW (2007) Material behaviors and mechanical features in friction stir welding process. Int J Adv Manuf Technol 35:86–100. https://doi.org/10.1007/s00170-006-0707-z
5. Ma ZY (2008) Friction stir processing technology: a review. Metall Mater Trans A 39:642–658. https://doi.org/10.1007/s11661-007-9459-0
6. Ma ZY, Mishra RS, Mahoney MW (2002) Superplastic deformation behaviour of friction stir processed 7075Al alloy. Acta Mater 50:4419–4430. https://doi.org/10.1016/S1359-6454(02)00278-1
7. Ma ZY, Xiao BL, Yang J, Feng AH (2010) Friction stir processing: a novel approach for microstructure refinement of magnesium alloys. Mater Sci Forum 638–642:1191–1196. https://doi.org/10.4028/www.scientific.net/MSF.638-642.1191
8. Mishra RS, Ma ZY, Charit I (2003) Friction stir processing: a novel technique for fabrication of surface composite. Mater Sci Eng A 341:307–310. https://doi.org/10.1016/S0921-5093(02)00199-5
9. Ma ZY, Sharma SR, Mishra RS (2006) Microstructural modification of As-cast Al-Si-Mg alloy by friction stir processing. Metall Mater Trans A Phys Metall Mater Sci 37:3323–3336. https://doi.org/10.1007/BF02586167
10. Hsu CJ, Kao PW, Ho NJ (2005) Ultrafine-grained Al-Al_2Cu composite produced in situ by friction stir processing. Scr Mater 53:341–345. https://doi.org/10.1016/j.scriptamat.2005.04.006
11. Hsu CJ, Chang CY, Kao PW et al (2006) Al-Al_3Ti nanocomposites produced in situ by friction stir processing. Acta Mater 54:5241–5249. https://doi.org/10.1016/j.actamat.2006.06.054
12. Chuang CH, Huang JC, Hsieh PJ (2005) Using friction stir processing to fabricate MgAlZn intermetallic alloys. Scr Mater 53:1455–1460. https://doi.org/10.1016/j.scriptamat.2005.08.019
13. Jafari J, Givi MKB, Barmouz M (2015) Mechanical and microstructural characterization of Cu/CNT nanocomposite layers fabricated via friction stir processing. Int J Adv Manuf Technol 78:199–209. https://doi.org/10.1007/s00170-014-6663-0
14. Kimura M, Kusaka M, Kaizu K et al (2016) Friction welding technique and joint properties of thin-walled pipe friction-welded joint between type 6063 aluminum alloy and AISI 304 austenitic stainless steel. Int J Adv Manuf Technol 82:489–499. https://doi.org/10.1007/s00170-015-7384-8
15. Nishhara T (2003) Development of friction stir forming. Mater Sci Forum 426-432:2971–2978
16. Nishihara T, Ito A (2005) Measurement of die temperature during friction stir forming. Weld World 49:22–26
17. Lazarevic S, Miller SF, Li J, Carlson BE (2013) Experimental analysis of friction stir forming for dissimilar material joining application. J Manuf Process 15:616–624. https://doi.org/10.1016/j.jmapro.2013.05.004
18. Lazarevic S, Ogata KA, Miller SF et al (2015) Formation and structure of work material in the friction stir forming process. J Manuf Sci Eng 137:51018. https://doi.org/10.1115/1.4030641
19. Ahuja Y, Ibrahim R, Paradowska A, Riley D (2015) Friction stir forming to fabricate copper-tungsten composite. J Mater Process Technol 217:222–231. https://doi.org/10.1016/j.jmatprotec.2014.11.024
20. Liu H, Zhao Y, Su X, et al (2013) Microstructural characteristics and mechanical properties of friction stir spot welded 2A12-T4 aluminum alloy. Adv Mater Sci Eng 2013:1–11. http://dx.doi.org/10.1155/2013/719306
21. Arul SG, Miller SF, Kruger GH et al (2008) Experimental study of joint performance in spot friction welding of 6111-T4 aluminium alloy. Sci Technol Weld Join 13:629–637. https://doi.org/10.1179/136217108X363900
22. Rao HM, Yuan W, Badarinarayan H (2015) Effect of process parameters on mechanical properties of friction stir spot welded magnesium to aluminum alloys. Mater Des 66:235–245. https://doi.org/10.1016/j.matdes.2014.10.065
23. Kumbhar NT, Bhanumurthy K (2012) Friction stir welding of Al 5052 with Al 6061 alloys. J Metall 2012:1–7. https://doi.org/10.1155/2012/303756
24. RajKumar V, VenkateshKannan M, Sadeesh P et al (2014) Studies on effect of tool design and welding parameters on the friction stir welding of dissimilar aluminium alloys AA 5052–AA 6061. Procedia Eng 75:93–97. https://doi.org/10.1016/j.proeng.2013.11.019
25. Park S-K, Hong S-T, Park J-H et al (2010) Effect of material locations on properties of friction stir welding joints of dissimilar aluminium alloys. Sci Technol Weld Join 15:331–336. https://doi.org/10.1179/136217110X12714217309696
26. C-S JEON, S-T HONG, Y-J KWON et al (2012) Material properties of friction stir spot welded joints of dissimilar aluminum alloys. Trans Nonferrous Met Soc China 22:s605–s613. https://doi.org/10.1016/S1003-6326(12)61772-5
27. Ramulu PJ, Narayanan RG, Kailas SV (2013) Forming limit investigation of friction stir welded sheets: influence of shoulder diameter and plunge depth. Int J Adv Manuf Technol 69:2757–2772. https://doi.org/10.1007/s00170-013-5245-x

28. Rahmi M, Abbasi M (2017) Friction stir vibration welding process: modified version of friction stir welding process. Int J Adv Manuf Technol 90:141–151. https://doi.org/10.1007/s00170-016-9383-9
29. Lakshminarayanan AK, Annamalai VE, Elangovan K (2015) Identification of optimum friction stir spot welding process parameters controlling the properties of low carbon automotive steel joints. J. Mater Res Technol 4(3):262–272
30. Awang M, Mucino VH (2010) Energy generation during friction stir spot welding (FSSW) of Al 6061-T6 plates. Mater Manuf Process 25:167–174. https://doi.org/10.1080/10426910903206758
31. Bozzi S, Helbert-Etter AL, Baudin T et al (2010) Influence of FSSW parameters on fracture mechanisms of 5182 aluminium welds. J Mater Process Technol 210:1429–1435. https://doi.org/10.1016/j.jmatprotec.2010.03.022
32. Ogata KA, Lazarevic S, Miller SF, Dissimilar material joint strength and structure for friction stir forming, ASME International Manufacturing Science and Engineering Conference, Volume 2: Processing, Detroit, Michigan, USA, June 9–13, 2014, pp.V002T02A076, https://doi.org/10.1115/MSEC2014-4044